



## Quantification of fossil fuel CO<sub>2</sub> from combined CO, δ<sup>13</sup>CO<sub>2</sub> and Δ<sup>14</sup>CO<sub>2</sub> observations

Jinsol Kim<sup>1</sup>, John B. Miller<sup>2</sup>, Charles E. Miller<sup>3</sup>, Scott J. Lehman<sup>4</sup>, Sylvia E. Michel<sup>4</sup>, Vineet Yadav<sup>3</sup>, Nick E. Rollins<sup>1</sup>, and William M. Berelson<sup>1</sup>

- 5 <sup>1</sup>Department of Earth Sciences, University of Southern California, Los Angeles, CA 90089, USA  
<sup>2</sup>Oceanic and Atmospheric Administration Global Monitoring Laboratory, Boulder, CO 80305, USA  
<sup>3</sup>Jet Propulsion Laboratory, California Institute of Technology, Pasadena, CA 91109, USA  
<sup>4</sup>Institute of Arctic and Alpine Research, University of Colorado, Boulder, CO 80309, USA

*Correspondence to:* Jinsol Kim (jinsolki@usc.edu)

10 **Abstract.** We present a new method for partitioning observed CO<sub>2</sub> enhancements (CO<sub>2</sub>xs) into fossil and biospheric fractions (C<sub>ff</sub> and C<sub>bio</sub>) based on measurements of CO and δ<sup>13</sup>CO<sub>2</sub>, complemented by flask-based Δ<sup>14</sup>CO<sub>2</sub> measurements. This method additionally partitions the fossil fraction into natural gas and petroleum fractions (when coal combustion is insignificant). Although here we apply the method only to discrete flask air measurements, the advantage of this  
15 method (CO and δ<sup>13</sup>CO<sub>2</sub>-based method) is that CO<sub>2</sub>xs partitioning can be applied at high frequency when continuous measurements of CO and δ<sup>13</sup>CO<sub>2</sub> are available. High frequency partitioning of CO<sub>2</sub>xs into C<sub>ff</sub> and C<sub>bio</sub> has already been demonstrated using continuous measurements of CO (CO-based method) and Δ<sup>14</sup>CO<sub>2</sub> measurements from flask air samples. Relative to calculating CO<sub>2</sub>ff directly from Δ<sup>14</sup>CO<sub>2</sub>, we find that the uncertainty in CO<sub>2</sub>ff estimated from the CO and  
20 δ<sup>13</sup>CO<sub>2</sub>-based method averages 3.2 ppm which is significantly less than the CO-based method which has an average uncertainty of 4.8 ppm. Using measurements of CO, δ<sup>13</sup>CO<sub>2</sub> and Δ<sup>14</sup>CO<sub>2</sub> from flask air samples at three sites in the greater Los Angeles region, we find large contributions of biogenic sources that vary by season. On a monthly average, the biogenic signal accounts for  
25 contributions in summer due to net respiration and net photosynthesis, respectively. Partitioning CO<sub>2</sub>ff into petroleum and natural gas combustion fractions reveals that the largest contribution of natural gas combustion generally occurs in summer, which is likely related to increased electricity generation in LA power plants for air-conditioning.



## 1 Introduction

The world's cities account for up to 70 % of global greenhouse gas (GHG) emissions, while covering less than 2 % of the Earth's surface (IPCC, 2014). Cities around the world have started implementing mitigation strategies to reduce carbon dioxide (CO<sub>2</sub>) emissions and collaborate with  
35 each other in organizations such as the C40 Cities Climate Leadership Group (<https://www.c40.org/>) and the Global Covenant of Mayors for Climate and Energy (<https://www.globalcovenantofmayors.org/>). To support urban efforts, monitoring systems are necessary to evaluate and verify reductions attributable to specific mitigation strategies.

Current understanding of anthropogenic CO<sub>2</sub> emissions mainly derives from methods that estimate  
40 aggregate emissions in a domain using economic statistics such as total fuel sales. These “bottom-up” methods provide specific location and process information that rely on mapping the source-specific emission factors and measurements of activities (e.g., McDonald et al. 2014; Gurney et al. 2019; Gately and Hutyra 2017). In contrast, more recently “top-down” methods that quantify emissions from measurements of atmospheric CO<sub>2</sub> have been used to estimate emissions. These  
45 top-down approaches typically use either a mass balance technique where an initial estimate is not required (e.g., Heimbürger et al. 2017; Ahn et al. 2020) or an inverse/data assimilation approach where observations and a prior map of emissions are combined to generate a best estimate (e.g., Sargent et al. 2018; Turner et al. 2020; Lauvaux et al. 2016, 2020).

To estimate anthropogenic CO<sub>2</sub> emissions using top-down method, it is crucial to separate the  
50 fossil fuel signals from the biogenic signals, which can vary from negative (uptake) to positive (emission) across the annual cycle. Recent analyses of urban CO<sub>2</sub> suggest that biogenic emissions and uptake have significant magnitudes relative to fossil fuel fluxes, especially during the growing season (Sargent et al. 2018; Vogel et al. 2019; Miller et al. 2020). Previous top-down studies used biosphere models to estimate biogenic fluxes and then determine the balance of emissions  
55 attributable to fossil fuel combustion (Sargent et al. 2018; Turner et al. 2020; Lauvaux et al. 2020). However, even with recent improvements in biosphere models (Wu et al. 2021; Gourdjji et al. 2022) the actual magnitude and variability of these fluxes are still not well constrained (Hardiman et al. 2017), potentially leading to unknown observational bias in the associated estimates of fossil fuel derived emissions.

60 Radiocarbon (<sup>14</sup>CO<sub>2</sub>) provides the ability to separate biogenic and anthropogenic CO<sub>2</sub> fluxes and mole fractions from an observational point of view (e.g. Levin, 2003; Turnbull 2006).



Observational methods rely on the fact that fossil fuels and the resultant CO<sub>2</sub> produced during combustion are completely devoid of <sup>14</sup>C (i.e.,  $\Delta^{14}\text{C}_{\text{ff}} = -1000\text{‰}$  on the widely used Delta scale). Measurements of  $\Delta^{14}\text{CO}_2$ , acquired at time scales of weeks to months, allow quantification of seasonal variations in biogenic and fossil contributions to the atmospheric CO<sub>2</sub> mole fraction (e.g., Djuricin et al. 2010; Miller et al. 2012; Turnbull et al. 2015). <sup>14</sup>C methods typically require air sample collection, preparation and analysis via accelerator mass spectrometry which limits the number of measurements, although a number of promising optical methods for in situ <sup>14</sup>CO<sub>2</sub> measurement at natural abundance are currently being developed (Fleisher et al. 2017; Genoud et al. 2019; McCartt and Jiang 2022).

On the other hand, carbon monoxide (CO) is a widely used tracer that can be measured continuously in situ using high-precision optical analyzers (e.g., Vogel et al. 2010; Newman et al. 2013; Turnbull et al. 2015). CO is often co-emitted with fossil fuel CO<sub>2</sub> (CO<sub>2ff</sub>) during incomplete combustion. If the CO<sub>x</sub>:CO<sub>2ff</sub> ratio ( $R_{\text{ff}}$ , where CO<sub>x</sub> is the CO enhancement above background) is well constrained, continuous CO measurements combined with  $R_{\text{ff}}$  can provide an estimate of continuous CO<sub>2ff</sub>. However, this approach is challenging because  $R_{\text{ff}}$  at a site may vary significantly on timescales ranging from hours to years (Levin and Karstens 2007; Vogel et al. 2010). CO:CO<sub>2</sub> emission ratio can vary by sources depending on the carbon content of the fuel and combustion conditions. Due to the impacts of atmospheric transport at a given observation site and the variability in the source combination in time and space,  $R_{\text{ff}}$  also varies in time and space. Vardag et al. (2015) proposed dividing fossil fuel emissions further into two groups that may display less variability in CO:CO<sub>2</sub> emission ratio. If one group is well constrained by CO and the other by <sup>13</sup>CO<sub>2</sub>, each group can be identified by combining CO and <sup>13</sup>CO<sub>2</sub> observations. Vardag et al. focused on separating traffic from non-traffic emissions, or biofuel emissions from the other fossil fuel emissions. However, no significant benefit of combining CO and <sup>13</sup>CO<sub>2</sub> was found because traffic and biofuel CO<sub>2</sub> do not produce distinct CO:CO<sub>2</sub> emission ratio or <sup>13</sup>CO<sub>2</sub> isotopic signatures compared to the other CO<sub>2ff</sub> source terms.

Here, we differentiate CO<sub>2</sub> signals from biogenic, petroleum and natural gas sources by combining CO,  $\delta^{13}\text{CO}_2$ , and  $\Delta^{14}\text{CO}_2$  measurements. The combination of  $\Delta^{14}\text{CO}_2$  and  $\delta^{13}\text{CO}_2$  has been used previously to distinguish biogenic, petroleum and natural gas signals for air sampling events (Lopez et al. 2013; Djuricin et al. 2010) and at seasonal scale (Newman et al. 2016). In contrast, the combination of CO and  $\delta^{13}\text{CO}_2$ , which can both be measured at high frequency, enables source



partitioning at higher temporal resolution. We demonstrate the agreement between the existing  $\Delta^{14}\text{CO}_2$ ,  $\delta^{13}\text{CO}_2$  and newly proposed CO,  $\delta^{13}\text{CO}_2$  methods. This establishes the utility of the CO  
95 and  $\delta^{13}\text{CO}_2$  in partitioning  $\text{CO}_2$ s into fossil fuel and biogenic components, with further partitioning of fossil fuel sources into petroleum and natural gas sources, in the Los Angeles megacity.

## 2 Methods

Here, we describe two methods for separating fossil fuel and biogenic components from  
100 atmospheric  $\text{CO}_2$  measurements in the complex urban environment of the Los Angeles megacity (LA). Section 2.2 describes our application of the method already described by Newman et al. (2016) using  $\Delta^{14}\text{CO}_2$  and  $\delta^{13}\text{CO}_2$  observations. The details of the new method utilizing CO and  $\delta^{13}\text{CO}_2$  measurements are described in section 2.3. Briefly, we take advantage of the fact that the combination of the CO: $\text{CO}_2$  emission ratio and the  $^{13}\text{C}$  isotopic signature reveal a very distinct  
105 pattern for biogenic, petroleum and natural gas sources. However, this approach requires knowledge of the CO: $\text{CO}_2$  emission ratio and the isotopic signature of each source. We apply isotopic signatures reported by previous studies, and CO: $\text{CO}_2$  emission ratios are determined for LA using measurements of CO,  $\delta^{13}\text{CO}_2$  and  $\Delta^{14}\text{CO}_2$  from flask samples. Flask measurements are described in section 2.1 and the source apportionment from  $\Delta^{14}\text{CO}_2$  and  $\delta^{13}\text{CO}_2$  observations,  
110 which is used to derive CO: $\text{CO}_2$  emission ratios for each source, is described in section 2.2.

### 2.1 Measurements

We use measurements from air samples collected at 2 p.m. local standard time at three existing Los Angeles Megacity Carbon Project sites: University of Southern California (USC), California State University, Fullerton (FUL), and Granada Hills (GRA) (Miller et al. 2020). Air samples were  
115 collected from November 2014 to March 2016 using National Oceanic and Atmospheric Administration (NOAA) programmable flask packages (PFPs) and programmable compressor packages (Sweeney et al. 2015). The samples were sent back to the NOAA Global Monitoring Laboratory where greenhouse gases including  $\text{CO}_2$  as well as CO mole fractions were measured using NOAA's high-precision/high-accuracy greenhouse gas measurement system (Sweeney et al.  
120 2015). After the measurement, residual air is extracted from PFP flasks and  $\text{CO}_2$  is isolated for  $^{14}\text{C}$



measurement using established cryogenic and mass spectrometric techniques (Lehman et al. 2013). Samples are purified, graphitized and packed into individual targets at the University of Colorado, Boulder, Institute of Arctic and Alpine Research (INSTAAR) and then sent to the University of California, Irvine, Keck Accelerator Mass Spectrometry Facility for high- precision  $\Delta^{14}\text{C}$  measurement. One-sigma measurement uncertainty is  $\sim 1.8$  ‰, equivalent to  $\sim 1.2$  parts per million (ppm) of recently added fossil fuel- $\text{CO}_2$ .  $\delta^{13}\text{CO}_2$  in PFP samples is measured by dual inlet isotope ratio mass spectrometry with a precision of approximately 0.02 ‰ at the INSTAAR Stable Isotope Laboratory (Vaughn et al. 2004; Sweeney et al. 2015)

Enhancement of each species is defined relative to a time-dependent background level, which is based on nighttime (2 AM local standard time) measurements made at Mount Wilson Observatory (MWO; Fig. 1) located at 1,670 m above sea level. Nighttime air at MWO generally represents the relatively clean, well-mixed free troposphere since polluted LA Basin boundary layer air has typically descended back into the basin by this time. After an additional step of filtering obvious outliers corresponding to pollution events indicated by anomalously elevated values were interpolated to the time of observations within the LA Basin by fitting curves to the screened MWO data (Fig. 2). A further analysis of associated CO measurements indicates that background reconstructed using nighttime air samples from MWO is representative of clean background air coming from either on- or off-shore (Miller et al. 2020).

## 2.2 Partitioning $\text{CO}_2$ signals using flask-based $\Delta^{14}\text{CO}_2$ and $\delta^{13}\text{CO}_2$ measurements

Our general approach to distinguishing  $\text{CO}_2$  signals from biogenic, petroleum and natural gas sources using  $\Delta^{14}\text{CO}_2$  and  $\delta^{13}\text{CO}_2$  follows the procedure described by Newman et al. (2016). Following previous derivations (e.g., Turnbull et al, 2006; Miller et al. 2020), we start with the definition for  $\text{CO}_2\text{ff}$  which is based on mass balances for the atmospherically conserved quantities  $\Delta^{14}\text{C}\times\text{CO}_2$  and  $\text{CO}_2$ :

$$C_{ff} = \frac{C_{obs}(\Delta_{obs}-\Delta_{bkg})}{(\Delta_{ff}-\Delta_{bkg})} - \frac{C_r(\Delta_r-\Delta_{bkg})}{(\Delta_{ff}-\Delta_{bkg})} \quad (1)$$

Measured  $\text{CO}_2$  mole fractions and  $\Delta^{14}\text{C}$  values are abbreviated as  $C$  and  $\Delta$ . Subscripts ‘obs’, ‘bkg’, ‘ff’ and ‘r’ represent observations, background, fossil fuel, and respiration, respectively.  $\Delta_{ff}$  is equal to  $-1000$  ‰. As in the Miller et al. (2020) study focusing on LA, we estimate the value of



the small respiratory term,  $-Cr(\Delta r - \Delta bkg)/(\Delta ff - \Delta bkg)$ , as 0.25 ppm. The overall uncertainty of  
150  $C_{ff}$  for LA measurements during 2015 is approximately 1.2 ppm, which includes 100%  
uncertainty assigned to the respiratory term.  $C_{ff}$  and  $C_{bio}$  ( $C_{bio} = C_{xs} - C_{ff}$ ) are calculated for all  
available flask air samples during the 2014 – 2016 sampling period, a frequency of approximately  
three times per week at each of the three sites.

$C_{ff}$  is then separated into signals from petroleum and natural gas combustion using  $^{13}C:^{12}C$  ratios  
155 ( $\delta^{13}C$  as defined by standard isotopic definition) measured on the same air samples. First, the flux  
weighted-mean  $\delta^{13}C$  signature of all sources located in the observation footprints ( $\delta_{src}$ ) is  
determined on a sample-by-sample basis using the combined mass balances for  $\delta^{13}C \times CO_2$  and  
 $CO_2$ :

$$\delta_{src} = \frac{\delta_{obs} \times C_{obs} - \delta_{bkg} \times C_{bkg}}{C_{obs} - C_{bkg}} \quad (2)$$

160 where  $\delta$  is short-hand for  $\delta^{13}CO_2$ . The uncertainties in  $C_{obs}$ ,  $C_{bkg}$ ,  $\delta_{obs}$ , and  $\delta_{bkg}$  are 0.1 ppm, 1.5  
ppm, 0.02 ‰, and 0.08 ‰, respectively. The “obs” uncertainties are measurement uncertainties,  
while the “bkg” uncertainties are determined as the standard deviation of the difference between  
the observations and their smoothed curve representation at MWO. The median uncertainty in  $\delta_{src}$   
is 3.0 ‰ and is calculated by propagating the uncertainties listed above, including covariance  
165 between  $\delta^{13}C$  and  $\delta^{13}C \times CO_2$ .

We combine  $C_{ff}$  (eq. 1) and  $\delta_{src}$  (eq. 2) to determine the  $\delta^{13}C$  signature of fossil fuel emissions,  
 $\delta_{ff}$ :

$$\delta_{src} = \delta_{ff} \times f_{ff} + \delta_{bio} \times (1 - f_{ff}) \quad (3)$$

Rearranging yields:

$$170 \quad \delta_{ff} = \frac{\delta_{src} - \delta_{bio} \times (1 - f_{ff})}{f_{ff}} \quad (4)$$

where  $f$  is the fraction. Following Newman et al. (2016), we take the isotopic signature of  
biospheric  $CO_2$  fluxes ( $\delta_{bio}$ ) to be  $-26.6 \pm 0.5$  ‰ based on the analysis of Northern Hemisphere  
mid-latitude  $CO_2$  and  $\delta^{13}C$  observations (Bakwin et al. 1998), which reflects the predominance of  
 $C_3$  photosynthesis. However, because LA turfgrasses, which could account for a significant  
175 fraction of urban  $CO_2$  fluxes [Miller, 2020], are often  $C_4$  species (e.g., Bermuda and Buffalo



grasses), we also conduct tests using  $\delta_{bio} = -20$  ‰, representing a C3/C4 mix (see Fig. S1).  $f_{ff}$  is the fraction of  $C_{ff}$  in  $C_{xs}$ , i.e.,  $C_{ff}/C_{xs}$ , and  $1 - f_{ff} = f_{bio}$ . Lastly, the proportion of  $C_{ff}$  emitted by petroleum (pet) and natural gas (ng) combustion,  $f_{pet}$  and  $f_{ng}$ , are calculated from the values of  $\delta_{ff}$ :

$$180 \quad \delta_{ff} = \delta_{pet} \times f_{pet/ff} + \delta_{ng} \times (1 - f_{pet/ff}) \quad (5)$$

$$f_{pet/ff} = \frac{\delta_{ff} - \delta_{ng}}{\delta_{pet} - \delta_{ng}} \quad (6)$$

We use values of  $-25.5 \pm 0.5$  ‰ for  $\delta_{pet}$  and  $-40.2 \pm 0.5$  ‰ for  $\delta_{ng}$  (Newman et al. 2008);  $f_{pet} = f_{ff} \times f_{pet/ff}$ , and  $f_{ng} = f_{ff} \times f_{ng/ff}$ , where  $f_{ng/ff} = 1 - f_{pet/ff}$ . We use temporally constant  $\delta^{13}\text{C}$  signatures for petroleum, natural gas and biogenic sources (and sinks), although with  
185 additional processed-based information, this assumption could be relaxed in the future. Note that although pet, ng, and bio signatures are fixed, both  $\delta_{src}$  and  $\delta_{ff}$  vary with time, meaning that  $f_{bio}$ ,  $f_{pet}$  and  $f_{ng}$  all vary at the frequency of the air sampling.

### 2.3 Partitioning CO<sub>2</sub> signals using CO and $\delta^{13}\text{CO}_2$ measurements

Although we can determine  $f_{bio}$ ,  $f_{pet}$  and  $f_{ng}$  at the frequency of discrete flask sampling events  
190 using the method described in Section 2.2, here we describe how comparable CO<sub>2</sub>s fractions can in theory be determined at high frequency using continuous measurements of CO and  $\delta^{13}\text{CO}_2$ . To evaluate the method, we compute the relative contributions of biogenic, petroleum and natural gas sources to CO<sub>2</sub>s using flask air CO and  $\delta^{13}\text{CO}_2$  measurements and compare these to values obtained using the  $\Delta^{14}\text{CO}_2$ -guided approach for the same samples by applying the following  
195 system of equations:

$$R_{src} = R_{bio} \times f_{bio} + R_{pet} \times f_{pet} + R_{ng} \times f_{ng} \quad (7)$$

$$\delta_{src} = \delta_{bio} \times f_{bio} + \delta_{pet} \times f_{pet} + \delta_{ng} \times f_{ng} \quad (8)$$

$$1 = f_{bio} + f_{pet} + f_{ng} \quad (9)$$

$R_{src}$  represents the CO/CO<sub>2</sub> ratio of the total source, which is the observed CO<sub>x</sub>s/CO<sub>2</sub>s ratio, and  
200 we use  $R$  to refer to the CO/CO<sub>2</sub> emission ratios of individual CO<sub>2</sub>s components (bio, pet, and ng). For now, we assume that  $R$  of each source are constant over a year-long period and over the



greater LA region (discussed in Section 3.2); especially with high frequency CO and  $\delta^{13}\text{C}_{\text{CO}_2}$  measurements, this assumption could easily be relaxed (discussed in Section 3.3).

205  $R$  values and  $\delta^{13}\text{C}$  signatures for bio, pet, and ng are needed to solve Eqs. 7-9.  $\delta^{13}\text{C}$  signatures are specified in section 2.2;  $R$  values are obtained via multiple linear regression of Eq. 7 using observed  $R_{\text{src}}$  and  $f$  values determined using  $\Delta^{14}\text{C}$  and  $\delta^{13}\text{C}$  of  $\text{CO}_2$  measurements as described in Section 2.2. Then we solve Eqs. 7-9 for new  $f$  values,  $f'$ . This new  $\text{CO}_2\text{s}$  partitioning (i.e.,  $f'_{\text{bio}}$ ,  $f'_{\text{pet}}$ ,  $f'_{\text{ng}}$ ) based on CO and  $\delta^{13}\text{C}_{\text{CO}_2}$  observations is used to calculate new values of  $C_{ff}$  and  $C_{\text{bio}}$  (i.e.,  $C'_{ff}$  and  $C'_{\text{bio}}$ ).

## 210 3 Results and Discussion

### 3.1 Contribution of biogenic, petroleum and natural gas sources in $\text{CO}_2$ excess

We calculated the fractional contribution of petroleum, natural gas, and biospheric fluxes to total  $\text{CO}_2\text{s}$  each month from April 2015 to March 2016 using  $\Delta^{14}\text{C}_{\text{CO}_2}$  and  $\delta^{13}\text{C}_{\text{CO}_2}$  observations recorded at FUL, USC and GRA. The results are given in Table S1 and presented in Figure 3. 215 Figure 4 presents the results in terms of the relative  $\text{CO}_2\text{s}$  contribution from each source at each site. We observe seasonal variation in  $\text{CO}_2\text{s}$  from each source. Fossil fuel is the dominant  $\text{CO}_2$  emissions source at each site which agrees with the findings of Newman et al. (2016) and Miller et al. (2020). Annually averaged across all three sites, biogenic emissions account for 6 % of  $\text{CO}_2\text{s}$ . Biogenic emissions are larger and positive in winter and smaller and negative in summer, 220 indicating winter respiration and uptake in summertime, generally consistent with the results of Miller et al. (2020). Note that in this study, we do not partition  $C_{\text{bio}}$  into an urban biosphere component and other components related to the oxidation of biogenic carbon including ethanol added to gasoline, and human and other animal food and waste (which can only be positive and are unlikely to vary much seasonally). If, as in Miller et al. (2020), we accounted for the always 225 positive ethanol, food, and waste signals, we would likely observe similarly large seasonal drawdown associated with urban vegetation.

We also observe spatial differences: The USC site exhibits a smaller contribution of the biosphere (3 % of annual average  $\text{CO}_2$  excess) compared to FUL and GRA (9 % and 5 % of total  $\text{CO}_2$  excess, respectively). However, these modest annual average biospheric contributions mask significant





230 seasonal activity. On a monthly basis, maximum positive biogenic contribution is observed in  
November at 25, 26, and 22 % at USC, FUL, and GRA (percentage of total CO<sub>2</sub> excess,  
respectively). And the maximum negative contribution, driven by net photosynthesis, is observed  
in July with values of -22, -13, and -12 % at USC, FUL, and GRA (percentage of total CO<sub>2</sub> excess,  
respectively).

235 Network average  $C_{ff}$  is  $11.0 \pm 14.5$  ppm in winter (November-February; median and standard  
deviation) and  $12.2 \pm 6.6$  ppm in summer (May-August). No significant difference is observed in  
winter and summer  $C_{ff}$ . This corresponds to the seasonality in Hestia-LA emissions, which  
indicates  $C_{ff}$  inputs are only 3 % higher in winter. High variability observed in wintertime  $C_{ff}$   
agrees with Miller et al. (2020) which is likely caused by increased temperature inversion trapping  
240 as the cold ground surface in winter cools the air layer right above the ground. While bottom-up  
fossil fuel emissions reveal little seasonality, the top-down seasonality of petroleum and natural  
gas (Fig. 4), which as fractions of  $C_{ff}$  should be largely independent of mixing, are clearly evident.  
The proportion of natural gas in fossil fuel signals are 40 % and 36 % in summer and 34 % and  
30% in winter at FUL and USC (Fig. 3). The increase in the natural gas contribution observed in  
245 summer can be explained by the increase in natural gas generated electricity in LA power plants  
to provide for air conditioning in summer (Newman et al. 2016; He et al. 2019). GRA, located  
northwest of USC by ~35 km without an electricity generation facility nearby, shows the opposite  
pattern (24 % in summer and 40 % in winter). This suggests the local influence of increased natural  
gas usage for heating in the winter.

### 250 3.2 R values of biogenic, petroleum and natural gas sources

Monthly, site-based  $R_{src}$  varies between 5.5 – 11.4 ppb ppm<sup>-1</sup> (Fig. 5), with a mean and standard  
deviation of  $8.2 \pm 1.6$  ppb/ppm (relative s.d. = 19 %). Greater variability is seen in  $R_{ff}$  (lower  
panel): mean and s.d. of  $9.6 \pm 2.1$  ppm (relative s.d. = 22 %). To understand and predict the  
variation in  $R_{ff}$ , we further divide the fossil fuel emissions into petroleum and natural gas  
emissions. Applying the calculated  $f$  values from  $\Delta^{14}\text{CO}_2$  and  $\delta^{13}\text{CO}_2$  observations (Section 2.2.,  
255 Fig. 3), we solve Eq. 7 for each source's CO/CO<sub>2</sub> emission ratio,  $R$  (Table 1). Note that we exclude  
negative flask-based values of CO<sub>x</sub>s (and corresponding  $R_{src}$  values) and CO<sub>2ff</sub> (and  
corresponding  $f_{ff}$  values) as non-physical. Likewise, positive  $\delta_{src}$  values and  $f_{pet/ff}$  values (and



corresponding  $f_{pet}$  and  $f_{ng}$  values) outside the range of 0-1 are also excluded. A bootstrapping  
260 method is used to calculate the mean and uncertainty of possible CO/CO<sub>2</sub> ratios. The CO/CO<sub>2</sub>  
ratios of petroleum ( $R_{pet}$ ) and natural gas ( $R_{ng}$ ) combustion emissions are  $12.2 \pm 0.6$  ppb ppm<sup>-1</sup>  
and  $2.3 \pm 1.2$  ppb ppm<sup>-1</sup>, respectively. As discussed above, the proportion of natural gas in fossil  
fuel emissions is bigger in summer resulting in smaller  $R_{ff}$  in summer at FUL and USC. We find  
the value of  $1.8 \pm 0.8$  ppb ppm<sup>-1</sup> for  $R_{bio}$  which is non-zero because biofuel (mainly corn-based  
265 ethanol) in the gasoline in California with large CO/CO<sub>2</sub> ratio signal is included in the biogenic  
sources while respiratory CO/CO<sub>2</sub> ratios approach 0. A larger contribution of the biosphere with a  
low CO/CO<sub>2</sub> ratio in winter offsets the large  $R_{ff}$  lowering the variability in  $R_{src}$  at each site.

We compare our model-determined CO/CO<sub>2</sub> ratios of each source (Table 2) to bottom-up  
inventory-based estimates (Table 1). CO/CO<sub>2</sub> ratios of each source constrained from our model  
270 and observational data approach agree well with the bottom-up inventory-based estimates. Sources  
contributing a high percentage of CO<sub>2</sub> emissions strongly influence the total CO/CO<sub>2</sub> ratio. The  
CO/CO<sub>2</sub> ratio of petroleum combustion is greatly affected by on-road emissions and industrial  
emissions (contributing 28 % and 60 % of total petroleum CO<sub>2</sub> emissions). Natural gas is mostly  
dominated by non-mobile emissions (Electricity production, residential, commercial, and  
275 industrial, sequentially) resulting in low CO/CO<sub>2</sub> ratio.

### 3.3 Estimation of CO<sub>2</sub>ff based on CO and <sup>13</sup>CO<sub>2</sub> observations

Table 2 shows the CO/CO<sub>2</sub> ratio and  $\delta^{13}\text{C}$  signature of each source. The combination of the  $R$  and  
 $\delta$  signals reveal a distinct pattern for each source: the biosphere has low near-zero  $R$ , petroleum  
has high  $R$ , and natural gas has low  $R$ . Petroleum and biosphere CO<sub>2</sub> have similar  $\delta$  values,  
280 whereas natural gas has a very low  $\delta$ . By substituting these values into Eqs. 7-9,  $f'$  values are  
calculated, and then we calculate  $C'_{ff}$  by multiplying the sum of  $f'_{pet}$  and  $f'_{ng}$  by CO<sub>2</sub>xs  
measured every few days. We compare  $f'_{ff}$  and  $C'_{ff}$  to  $f_{ff}$  and  $C_{ff}$  (determined using <sup>14</sup>C  
observations) in Fig. 6. Assessment for each source is shown in Figure S2 and S3. The  $R^2$  values  
are 0.63 and 0.90 for  $f'_{ff}$  and  $C'_{ff}$ , respectively.

285 If  $R$  values are allowed to vary in time, it is likely to improve the precision of the method. We  
calculate the uncertainty in  $C'_{ff}$  for varying temporal resolutions of  $R$  (black solid line in Fig. 7).  
We find that the uncertainty increases when the size of the window increases from 1-week to 10-



week; in other words, allowing temporal variation in  $R$  improves the precision of the method. However, the uncertainty slightly decreases beyond the 10-week window. This is likely caused by  
290 the reduction in the error of  $R$  values (not shown) as the number of observations used to find  $R$  (by solving Eq. 7) increases. In summary, the ideal flask sampling frequency for this method would be higher than every 2 weeks. In cases where this is impossible, it is better to assume constant  $R$  values.

The uncertainty in  $C'_{ff}$  estimated using the CO-based method is also shown in Figure 7 (black  
295 dashed line). The CO-based method also provides improved precision of the method when flask sampling is available at higher frequency. However, the CO and  $\delta^{13}\text{CO}_2$ -based method shows greater confidence than the CO-based method for the whole range of adjusted temporal resolution in  $R$ . When using constant  $R$  values (temporal resolution of 50 weeks), the uncertainty is 3.2 ppm (the  $1\sigma$  standard deviation of differences between  $C_{ff}$  and  $C'_{ff}$ ) for the CO and  $\delta^{13}\text{CO}_2$ -based  
300 method, while it is 4.8 ppm for CO-based method. This improvement is likely associated with the additional information provided by  $\delta^{13}\text{CO}_2$  that constrains the effective  $R_{ff}$  and further separates fossil fuel sources into sub-categories (petroleum and natural gas sources).

#### 4 Conclusions

We present a CO and  $\delta^{13}\text{CO}_2$ -based method to estimate  $\text{CO}_2\text{ff}$  which is based on flask-based  
305  $\Delta^{14}\text{CO}_2$  measurements. We have applied the method to measurements from flask samples collected in the LA basin, every few days in the afternoon for more than one year (2015-16). The proposed method was assessed by comparing it to a more traditional  $\Delta^{14}\text{CO}_2$ -based method. CO and  $\delta^{13}\text{CO}_2$  approach can be applied to continuous measurements of  $\text{CO}_2$ , CO and  $\delta^{13}\text{CO}_2$  which can provide  $\text{CO}_2\text{ff}$  estimates at higher temporal resolution and with greater accuracy than previously applied  
310 CO-based methods.

We have analyzed three locations in the Los Angeles megacity, partitioning observed  $\text{CO}_2$  enhancements ( $\text{CO}_2\text{xs}$ ) into biogenic, petroleum and natural gas sources. We observed a substantial biogenic signal that varies from -14% to +25% of  $\text{CO}_2\text{xs}$  over the course of the year, with positive contributions in winter and negative contributions in summer due to net respiration  
315 and net photosynthesis, respectively. Furthermore, partitioning  $\text{CO}_2\text{ff}$  into petroleum and natural gas combustion fractions revealed that natural gas combustion has the largest contribution in



summer, potentially due to an increase in electricity generation at LA power plants for air conditioning.

320 **Data availability.** The data that support the findings of this study are available from JBM (john.b.miller@noaa.gov) upon request.

**Author contributions.** JK designed and executed the study. JBM, SJL, and SEM provided the data. JK prepared the manuscript with contributions from all co-authors

325

**Competing interests.** The authors declare that they have no conflict of interest.

## References

- Ahn, D. Y., J. R. Hansford, S. T. Howe, X. R. Ren, R. J. Salawitch, N. Zeng, M. D. Cohen, et al. 2020. “Fluxes of Atmospheric Greenhouse-Gases in Maryland (FLAGG-MD): Emissions of Carbon Dioxide in the Baltimore, MD-Washington, D.C. Area.” *Journal of Geophysical Research: Atmospheres* 125 (9): 1–23. <https://doi.org/10.1029/2019JD032004>.
- Bakwin, Peter S., Pieter P. Tans, James W.C. White, and Robert J. Andres. 1998. “Determination of the Isotopic ( $^{13}\text{C}/^{12}\text{C}$ ) Discrimination of Terrestrial Biology from a Global Network of Observations.” *Global Biogeochemical Cycles* 12 (3). <https://doi.org/10.1029/98GB02265>.
- 335 Djuricin, Sonja, Diane E. Pataki, and Xiaomei Xu. 2010. “A Comparison of Tracer Methods for Quantifying CO<sub>2</sub> Sources in an Urban Region.” *Journal of Geophysical Research* 115 (14): 1–13. <https://doi.org/10.1029/2009JD012236>.
- Fleisher, Adam J., David A. Long, Qingnan Liu, Lyn Gameson, and Joseph T. Hodges. 2017. “Optical Measurement of Radiocarbon below Unity Fraction Modern by Linear Absorption Spectroscopy.” *Journal of Physical Chemistry Letters* 8 (18). <https://doi.org/10.1021/acs.jpcclett.7b02105>.
- 340 Gately, C. K., and L. R. Hutyrá. 2017. “Large Uncertainties in Urban-Scale Carbon Emissions.” *Journal of Geophysical Research: Atmospheres* 122 (20): 11,242–11,260. <https://doi.org/10.1002/2017JD027359>.
- 345 Genoud, Guillaume, Johannes Lehmuskoski, Steven Bell, Vesa Palonen, Markku Oinonen, Mari Leena Koskinen-Soivi, and Matti Reinikainen. 2019. “Laser Spectroscopy for Monitoring



- of Radiocarbon in Atmospheric Samples.” *Analytical Chemistry* 91 (19).  
<https://doi.org/10.1021/acs.analchem.9b02496>.
- 350 Gourdj, Sharon M., Anna Karion, Israel Lopez-Coto, Subhomoy Ghosh, Kimberly L. Mueller,  
Yu Zhou, Christopher A. Williams, Ian T. Baker, Katharine D. Haynes, and James R.  
Whetstone. 2022. “A Modified Vegetation Photosynthesis and Respiration Model (VPRM)  
for the Eastern USA and Canada, Evaluated With Comparison to Atmospheric Observations  
and Other Biospheric Models.” *Journal of Geophysical Research: Biogeosciences* 127 (1).  
355 <https://doi.org/10.1029/2021JG006290>.
- Gurney, K. R., Risa Patarasuk, Jianming Liang, Yang Song, Darragh O’Keefe, Preeti  
Rao, James R. Whetstone, Riley M. Duren, Annmarie Eldering, and Charles E. Miller.  
2019. “The Hestia Fossil Fuel CO<sub>2</sub> Emissions Data Product for the Los Angeles Megacity  
(Hestia-LA).” *Earth System Science Data* 11: 1309–35. [https://doi.org/10.5194/essd-2018-](https://doi.org/10.5194/essd-2018-162)  
360 162.
- Hardiman, Brady S., Jonathan A. Wang, Lucy R. Hutyra, C. K. Gatley, Jackie M. Getson, and  
Mark A. Friedl. 2017. “Accounting for Urban Biogenic Fluxes in Regional Carbon  
Budgets.” *Science of the Total Environment* 592: 366–72.  
<https://doi.org/10.1016/j.scitotenv.2017.03.028>.
- 365 He, Liyin, Zhao-Cheng Zeng, Thomas J. Pongetti, Clare Wong, Jianming Liang, K. R. Gurney,  
Sally Newman, et al. 2019. “Atmospheric Methane Emissions Correlate With Natural Gas  
Consumption From Residential and Commercial Sectors in Los Angeles.” *Geophysical  
Research Letters* 46 (14): 8563–71. <https://doi.org/10.1029/2019gl083400>.
- Heimbürger, Alexie, Rebecca Harvey, Paul B. Shepson, Brian H. Stirm, Chloe Gore, J. C.  
370 Turnbull, Maria O. L. Cambaliza, et al. 2017. “Assessing the Optimized Precision of the  
Aircraft Mass Balance Method for Measurement of Urban Greenhouse Gas Emission Rates  
through Averaging.” *Elem Sci Anth* 5 (0): 26. <https://doi.org/10.1525/elementa.134>.
- Lauvaux, Thomas, K. R. Gurney, Natasha L. Miles, Kenneth J. Davis, Scott J. Richardson, Aijun  
Deng, Brian J. Nathan, et al. 2020. “Policy-Relevant Assessment of Urban CO<sub>2</sub> emissions.”  
375 *Environmental Science and Technology* 54 (16): 10237–45.  
<https://doi.org/10.1021/acs.est.0c00343>.
- Lauvaux, Thomas, Natasha L. Miles, Aijun Deng, Scott J. Richardson, Maria O. Cambaliza,  
Kenneth J. Davis, Brian Gaudet, et al. 2016. “High-Resolution Atmospheric Inversion of



- Urban CO<sub>2</sub> Emissions during the Dormant Season of the Indianapolis Flux Experiment (INFLUX).” *Journal of Geophysical Research* 121 (10): 5213–36.  
380 <https://doi.org/10.1002/2015JD024473>.
- Lehman, Scott J, John B. Miller, Chad Wolak, John Southon, Pieter P Tans, Stephen A Montzka, Colm Sweeney, et al. 2013. “Allocation of Terrestrial Carbon Sources Using 14 CO<sub>2</sub> : Methods, Measurement, and Modeling.” *Radiocarbon* 55 (3).  
385 <https://doi.org/10.1017/s0033822200048414>.
- Levin, Ingeborg, and Ute Karstens. 2007. “Inferring High-Resolution Fossil Fuel CO<sub>2</sub> Records at Continental Sites from Combined 14CO<sub>2</sub> and CO Observations.” *Tellus, Series B: Chemical and Physical Meteorology* 59 (2): 245–50. <https://doi.org/10.1111/j.1600-0889.2006.00244.x>.
- 390 Lopez, Morgan, M. Schmidt, M. Delmotte, A. Colomb, V. Gros, C. Janssen, S. J. Lehman, et al. 2013. “CO, NO<sub>x</sub> and 13CO<sub>2</sub> as Tracers for Fossil Fuel CO<sub>2</sub>: Results from a Pilot Study in Paris during Winter 2010.” *Atmospheric Chemistry and Physics* 13 (15): 7343–58. <https://doi.org/10.5194/acp-13-7343-2013>.
- McCartt, A. Daniel, and Jun Jiang. 2022. “Room-Temperature Optical Detection of 14CO<sub>2</sub> below the Natural Abundance with Two-Color Cavity Ring-Down Spectroscopy.” *ACS Sensors* 7 (11). <https://doi.org/10.1021/acssensors.2c01253>.  
395
- Mcdonald, Brian C., Zoe C. McBride, Elliot W. Martin, and Robert A. Harley. 2014. “High-Resolution Mapping of Motor Vehicle Carbon Dioxide Emissions.” *Journal of Geophysical Research: Atmospheres*, no. May: 5283–98.  
400 <https://doi.org/10.1002/2013JD021219>.Received.
- Miller, John B., Scott J. Lehman, Stephen A Montzka, Colm Sweeney, Benjamin R Miller, Anna Karion, Chad Wolak, et al. 2012. “Linking Emissions of Fossil Fuel CO<sub>2</sub> and Other Anthropogenic Trace Gases Using Atmospheric 14CO<sub>2</sub>.” *Journal of Geophysical Research: Atmospheres* 117. <https://doi.org/10.1029/2011JD017048>.
- 405 Miller, John B., Scott J. Lehman, Kristal R. Verhulst, Charles E. Miller, Riley M. Duren, Vineet Yadav, Sally Newman, and Christopher D. Sloop. 2020. “Large and Seasonally Varying Biospheric CO<sub>2</sub> Fluxes in the Los Angeles Megacity Revealed by Atmospheric Radiocarbon.” *Proceedings of the National Academy of Sciences of the United States of America* 117 (43): 26681–87. <https://doi.org/10.1073/pnas.2005253117>.



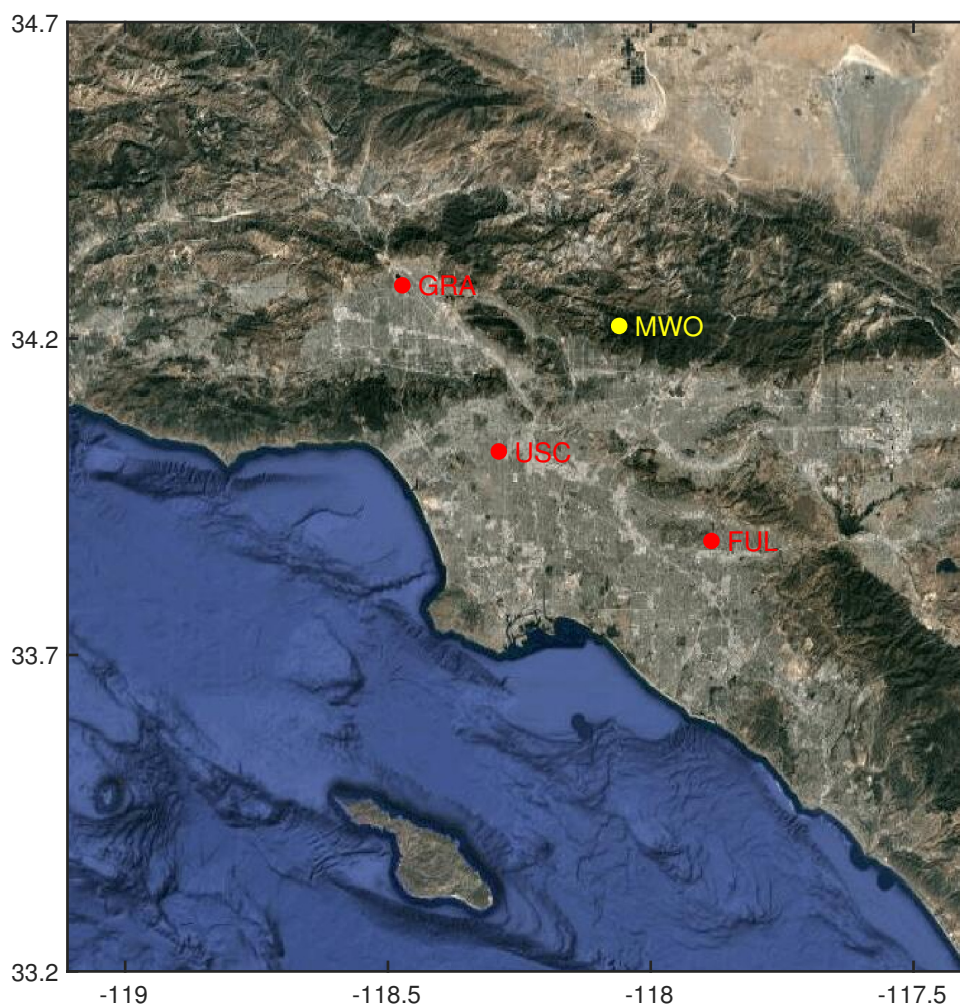
- 410 Newman, Sally, and S. Jeong. 2013. “Diurnal Tracking of Anthropogenic CO<sub>2</sub> Emissions in the Los Angeles Basin Megacity during Spring 2010.” *Atmospheric Chemistry and Physics*, 4359–72. <https://doi.org/10.5194/acp-13-4359-2013>.
- Newman, Sally, Xiaomei Xu, Hagit P. Affek, Edward Stolper, and Samuel Epstein. 2008. “Changes in Mixing Ratio and Isotopic Composition of CO<sub>2</sub> in Urban Air from the Los Angeles Basin, California, between 1972 and 2003.” *Journal of Geophysical Research Atmospheres* 113 (23): 1–15. <https://doi.org/10.1029/2008JD009999>.
- 415 Newman, Sally, Xiaomei Xu, K. R. Gurney, Ying Kuang Hsu, King Fai Li, Xun Jiang, Ralph F. Keeling, et al. 2016. “Toward Consistency between Trends in Bottom-up CO<sub>2</sub> Emissions and Top-down Atmospheric Measurements in the Los Angeles Megacity.” *Atmospheric Chemistry and Physics* 16 (6): 3843–63. <https://doi.org/10.5194/acp-16-3843-2016>.
- 420 Sargent, Maryann, Yanina Barrera, Thomas Nehrkorn, L. R. Hutyra, C. K. Gatley, Taylor Jones, Kathryn McKain, et al. 2018. “Anthropogenic and Biogenic CO<sub>2</sub> Fluxes in the Boston Urban Region.” *Proceedings of the National Academy of Sciences* 115 (29): 7491–96. <https://doi.org/10.1073/pnas.1803715115>.
- 425 Sweeney, Colm, Anna Karion, Sonja Wolter, Timothy Newberger, Doug Guenther, Jack A Higgs, Arlyn Elyzabeth Andrews, et al. 2015. “Seasonal Climatology of CO<sub>2</sub> across North America from Aircraft Measurements in the NOAA/ESRL Global Greenhouse Gas Reference Network.” *Journal of Geophysical Research : Atmospheres*, 5155–90. <https://doi.org/10.1002/2014JD022591>.Received.
- 430 Turnbull, J. C., Anna Karion, Kenneth J. Davis, Thomas Lauvaux, Natasha L. Miles, Scott J. Richardson, Colm Sweeney, et al. 2019. “Synthesis of Urban CO<sub>2</sub> Emission Estimates from Multiple Methods from the Indianapolis Flux Project (INFLUX).” *Environmental Science and Technology* 53 (1): 287–95. <https://doi.org/10.1021/acs.est.8b05552>.
- 435 Turnbull, J. C., Colm Sweeney, Anna Karion, Timothy Newberger, Scott J. Lehman, Pieter P. Tans, Kenneth J. Davis, et al. 2015. “Toward Quantification and Source Sector Identification of Fossil Fuel CO<sub>2</sub> Emissions from an Urban Area: Results from the INFLUX Experiment.” *Journal of Geophysical Research* 120 (1): 292–312. <https://doi.org/10.1002/2014JD022555>.
- 440 Turner, Alexander J., Jinsol Kim, Helen Fitzmaurice, Catherine Newman, Kevin Worthington, Katherine Chan, Paul Wooldridge, Philipp Köhler, Christian Frankenberg, and Ronald C.





- Cohen. 2020. “Observed Impacts of COVID-19 on Urban CO<sub>2</sub> Emissions.” *Geophysical Research Letters*, 2–10.
- Vardag, S. N., C. Gerbig, G. Janssens-Maenhout, and Ingeborg Levin. 2015. “Estimation of Continuous Anthropogenic CO<sub>2</sub>: Model-Based Evaluation of CO<sub>2</sub>, CO,  $\Delta^{13}\text{C}(\text{CO}_2)$  and  $\Delta^{14}\text{C}(\text{CO}_2)$  Tracer Methods.” *Atmospheric Chemistry and Physics* 15 (22): 12705–29. 445  
<https://doi.org/10.5194/acp-15-12705-2015>.
- Vaughn, B. H., John B. Miller, D. F. Ferretti, and J. W.C. White. 2004. “Stable Isotope Measurements of Atmospheric CO<sub>2</sub> and CH<sub>4</sub>.” In *Handbook of Stable Isotope Analytical Techniques*. <https://doi.org/10.1016/B978-044451114-0/50016-8>.
- 450 Vogel, Felix R., Matthias Frey, Johannes Staufer, Frank Hase, Grégoire Broquet, and Irène Xueref-remy. 2019. “XCO<sub>2</sub> in an Emission Hot-Spot Region : The COCCON Paris Campaign 2015.” *Atmospheric Chemistry and Physics* 19: 3271–85.
- Vogel, Felix R., Samuel Hammer, Axel Steinhof, Bernd Kromer, and Ingeborg Levin. 2010. “Implication of Weekly and Diurnal <sup>14</sup>C Calibration on Hourly Estimates of CO-Based 455  
Fossil Fuel CO<sub>2</sub> at a Moderately Polluted Site in Southwestern Germany.” *Tellus, Series B: Chemical and Physical Meteorology* 62 (5): 512–20. <https://doi.org/10.1111/j.1600-0889.2010.00477.x>.
- Wu, Dien, John C. Lin, Henrique F. Duarte, Vineet Yadav, Nicholas C. Parazoo, Tomohiro Oda, and Eric A. Kort. 2021. “A Model for Urban Biogenic CO<sub>2</sub> Fluxes: Solar-Induced 460  
Fluorescence for Modeling Urban Biogenic Fluxes (SMUrF V1).” *Geoscientific Model Development* 14 (6). <https://doi.org/10.5194/gmd-14-3633-2021>.





465

**Figure 1.** Map of the greater Los Angeles region. The three Los Angeles Megacity Carbon Project sites are marked in red and the Mount Wilson Observatory used to define background values are marked in yellow. Map data © Google Maps 2022.

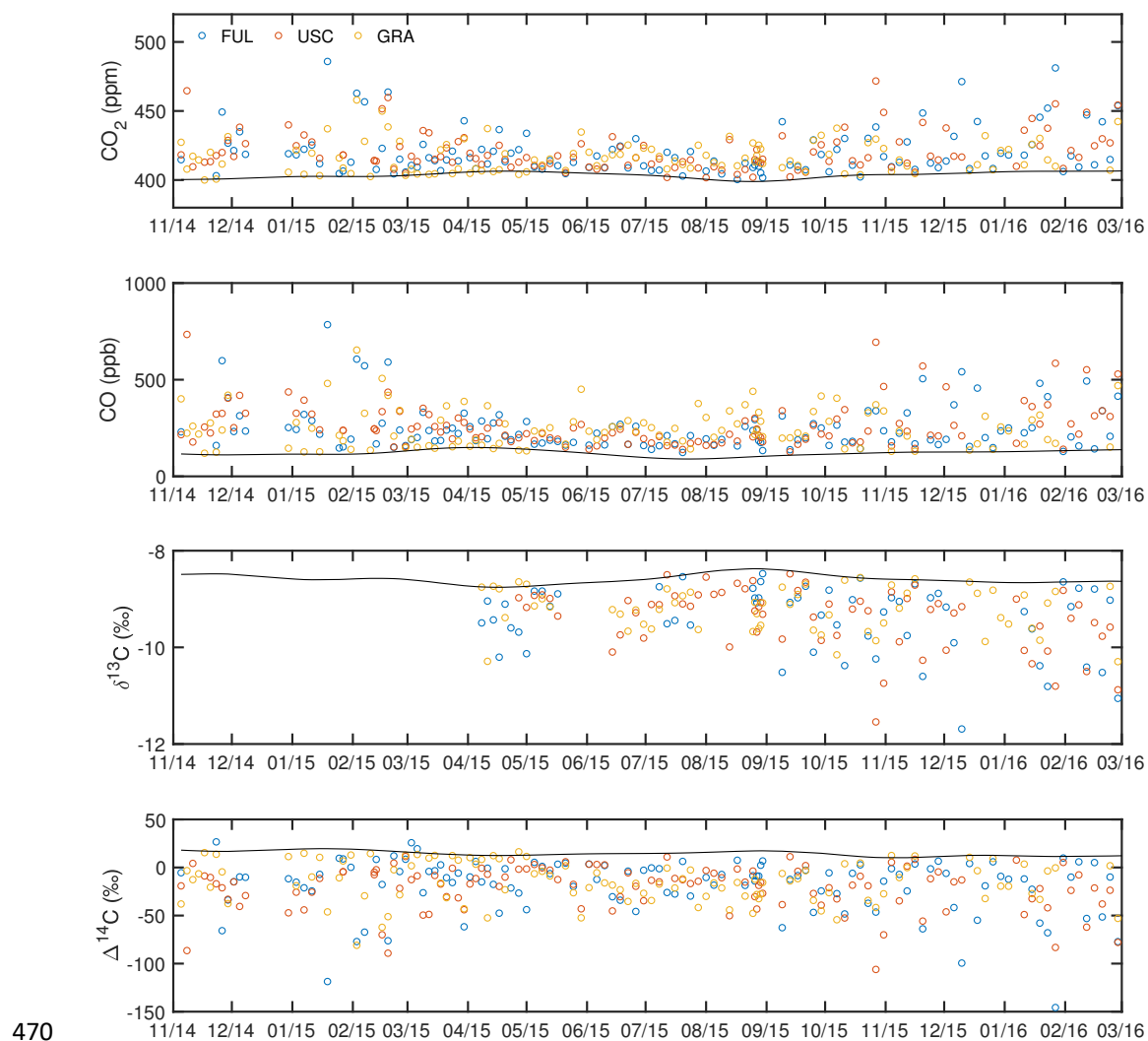
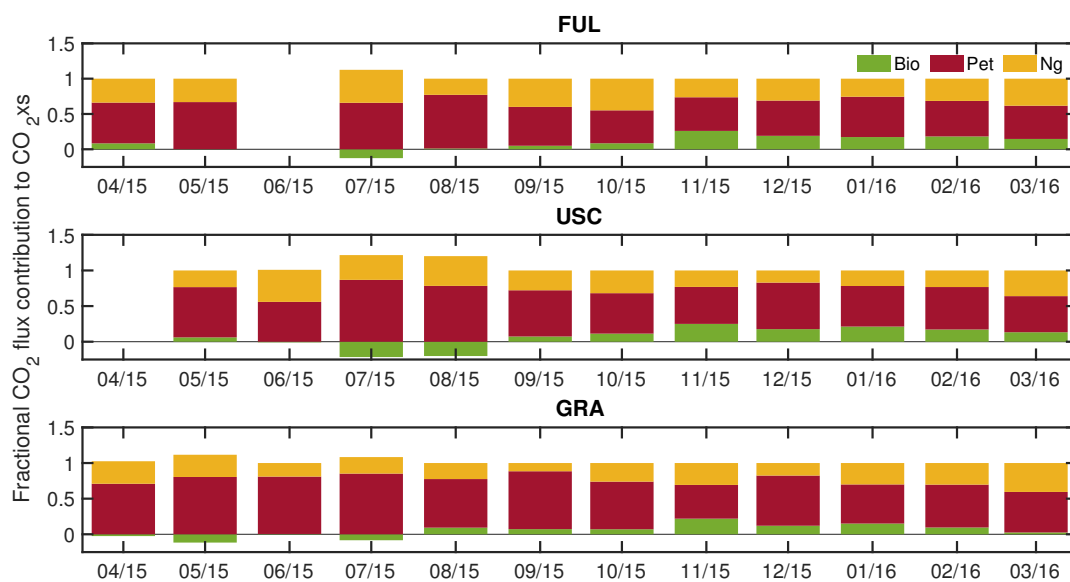


**Figure 2.** Timeseries of CO<sub>2</sub>, CO, δ<sup>13</sup>C, and Δ<sup>14</sup>C. Black line represents background values.

475

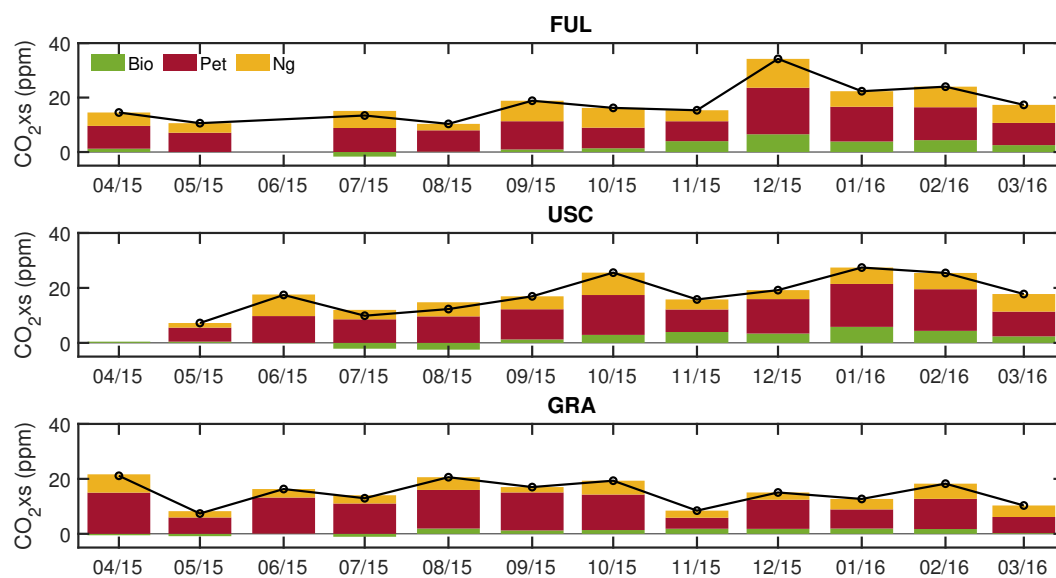
480



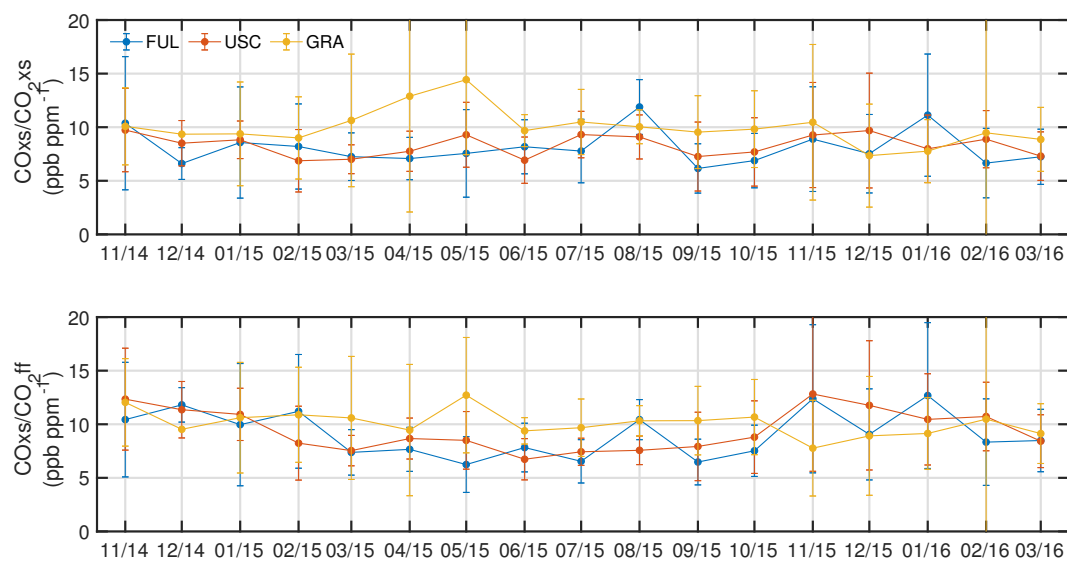
485

**Figure 3.** Monthly mean fractional contributions (f) of biosphere (green), petroleum (red), and natural gas (yellow) to CO<sub>2</sub>xs at each site, as determined from  $\Delta^{14}\text{C}$  and  $\delta^{13}\text{C}$  observations (Section 2.2). The sum of the fractions is one in each month.

490



495 **Figure 4.** Monthly mean CO<sub>2</sub>xs partitioned into biosphere (green), petroleum (red), and natural gas (yellow) signals, as determined from  $\Delta^{14}\text{C}$  and  $\delta^{13}\text{C}$  observations, at each site. The black marker indicates CO<sub>2</sub>xs.



500

**Figure 5.** Monthly variations in COxs/CO<sub>2</sub>xs (Rsrc) and COxs/CO<sub>2</sub>ff (Rff) at each site. COxs/CO<sub>2</sub>ff is calculated using <sup>14</sup>C observations.



505

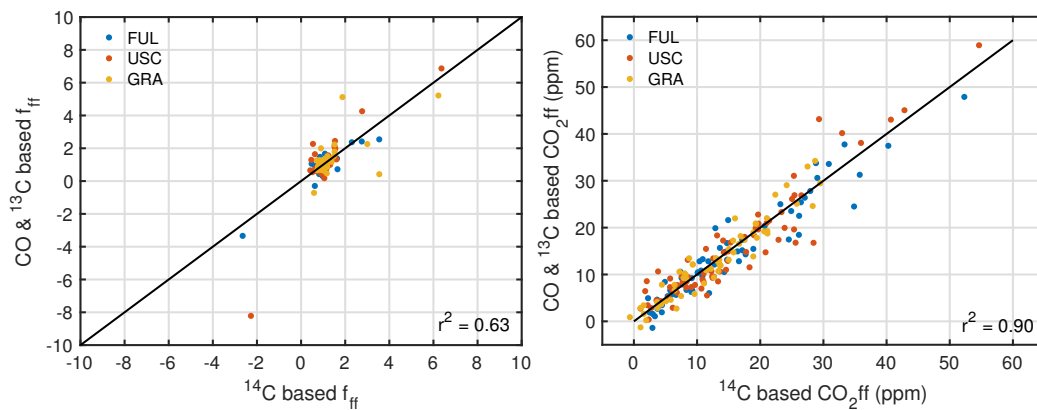


**Figure 6.** Comparison of  $f_{ff}$  and  $f'_{ff}$  (left) and  $C_{ff}$  and  $C'_{ff}$  (right). Black lines represent 1:1 relationships and different colors indicate different sites.

510

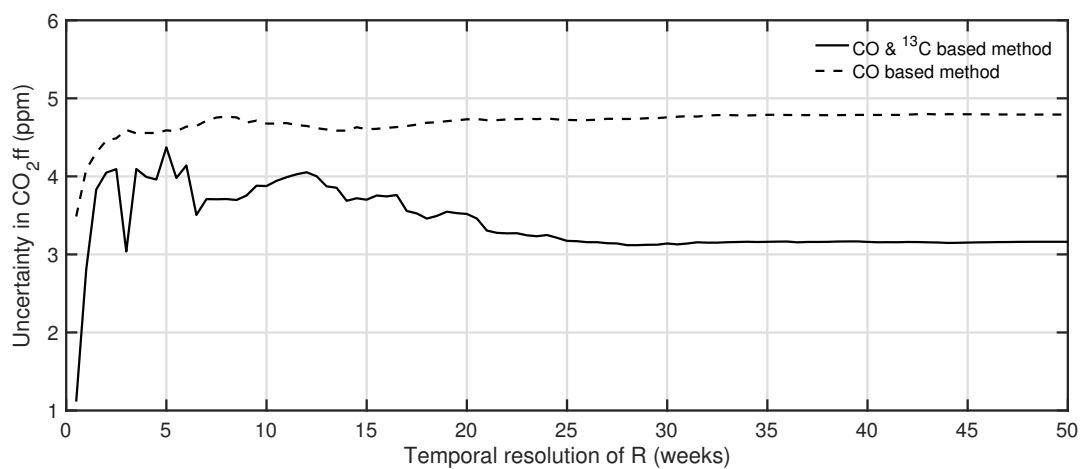


**Figure 7.** Uncertainty in  $C'_{ff}$  for varying temporal resolution of  $R$  ( $N$  weeks).  $R$  is determined for each data point solving Eq. 7 using  $\text{CO}$ ,  $^{13}\text{CO}_2$  and  $^{14}\text{CO}_2$  observations within a moving window of  $2N$  weeks. For  $\text{CO}$ -based method,  $R_{ff}$  is smoothed using a  $2N$  weeks moving window.



520

**Table 1.** Bottom-up CO<sub>2</sub> emission, CO emission, and R (CO/CO<sub>2</sub> ratio) estimates for each source sector and fuel type for LA basin based on the Vulcan 3.0 and the U.S. Environmental Protection Agency (EPA) National Emission Inventory for 2011 (NEI 2011) product. NEI 2011 is scaled by the emissions with fuel consumption dataset from the U.S. Energy Information Administration (EIA) State Energy Data System (SEDS) to estimate 2015 CO emissions.

	-----Petroleum-----			-----Natural Gas-----		
	CO <sub>2</sub> (MtC)	CO (MtC)	R = CO/CO <sub>2</sub> (ppb ppm <sup>-1</sup> )	CO <sub>2</sub> (MtC)	CO (MtC)	R = CO/CO <sub>2</sub> (ppb ppm <sup>-1</sup> )
Residential	0.06	<0.001	0.07	2.79	0.001	1.21
Commercial	0.67	<0.001	0.34	1.79	0.002	2.54
Industrial	9.79	<0.001	0.06	1.59	0.002	2.99
Electricity Production	0.37	<0.001	0.04	5.08	0.002	0.74
On-road	20.97	0.296	31.79	0	0	
Non-road	1.45	0.139	224.11	0.19	0.012	152.41
Airport	0.89	0.008	21.63	0	0	
Rail	0.47	0.002	11.94	0	0	
CMV	0.48	<0.001	3.26	0	0	
<b>Total</b>	<b>35.16</b>	<b>0.437</b>	<b>12.42</b>	<b>11.44</b>	<b>0.019</b>	<b>1.68</b>

525





**Table 2.** CO/CO<sub>2</sub> ratios (*R*) and δ<sup>13</sup>C signatures used to determine relative contribution of biogenic, petroleum and natural gas sources.

	Biosphere	Petroleum	Natural Gas
Bottom-up approach <i>R</i> (ppb ppm <sup>-1</sup> ) <sup>a</sup>		12.4	1.7
Top-down approach <i>R</i> (ppb ppm <sup>-1</sup> ) <sup>b</sup>	1.8 ± 0.8	12.2 ± 0.6	2.3 ± 1.2
δ <sup>13</sup> C (‰) <sup>c</sup>	-26.6 ± 0.5	-25.5 ± 0.5	-40.2 ± 0.5

530

<sup>a</sup>*R* calculated from Table 1. These values are not used for CO<sub>2</sub>xs partitioning and are for reference only.

<sup>b</sup>*R* calculated from CO, δ<sup>13</sup>CO<sub>2</sub> and Δ<sup>14</sup>CO<sub>2</sub> flask observations. These values are used in this study.

535 <sup>c</sup>δ<sup>13</sup>C from previous studies (Newman et al., 2008)